University of Kent

Kent Academic Repository

Nteroli, Gianni, Dasa, Manoj K, Messa, Giulia, Koutsikou, Stella, Bondu, Magalie M., Moselund, Peter M., Markos, Christos, Bang, Ole, Podoleanu, Adrian G. H. and Bradu, Adrian (2024) ***Development of a combined multi-spectral optoacoustic microscopy and optical coherence tomography imaging instrument for mapping multiple chromophores in biological tissues.*** **In: Proceedings Volume 13006 SPIE Photonics Europe. 13006. p. 42. SPIE**

Downloaded from

https://kar.kent.ac.uk/106796/ The University of Kent's Academic Repository KAR

The version of record is available from

https://doi.org/doi:10.1117/12.3017439

This document version

Author's Accepted Manuscript

DOI for this version

Licence for this version

CC BY (Attribution)

Additional information

Versions of research works

Versions of Record

If this version is the version of record, it is the same as the published version available on the publisher's web site. Cite as the published version.

Author Accepted Manuscripts

If this document is identified as the Author Accepted Manuscript it is the version after peer review but before type setting, copy editing or publisher branding. Cite as Surname, Initial. (Year) 'Title of article'. To be published in ***Title of Journal*** , Volume and issue numbers [peer-reviewed accepted version]. Available at: DOI or URL (Accessed: date).

Enquiries

If you have questions about this document contact ResearchSupport@kent.ac.uk. Please include the URL of the record in KAR. If you believe that your, or a third party's rights have been compromised through this document please see our Take Down policy (available from https://www.kent.ac.uk/guides/kar-the-kent-academic-repository#policies).

Development of a combined multi-spectral optoacoustic microscopy and optical coherence tomography imaging instrument for mapping multiple chromophores in biological tissues

Gianni Nteroli[a], Manoj K. Dasa[b], Giulia Messa[c], Stella Koutsikou[d], Magalie Bondu[b], Peter M. Moselund[b], Christos Markos[e], Ole Bang[e], Adrian Podoleanu[a], and Adrian Bradu[a*]

[a]Applied Optics Group, University of Kent, Canterbury, United Kingdom
[b]NKT Photonics A/S, Blokken 84, 3460 Birkerød, Denmark
[c]L'Institut du Cerveau et de la Moelle Epinière, Paris, France
[d]Medway School of Pharmacy, University of Kent, Chatham, United Kingdom
[e]DTU Fotonik, Technical University of Denmark, 2800 Kgs. Lyngby, Denmark.
* Corresponding author: g.nteroli@kent.ac.uk

ABSTRACT

This report presents a state-of-the-art multimodality imaging device that combines multi-spectral optoacoustic microscopy (OAM) and optical coherence tomography (OCT) to chart absorbers in live tadpoles (*Xenopus laevis*) accurately. The OAM channel captures maps of five internal contrast agents: melanin, hemoglobin, collagen, glucose, and lipids. A novel method was developed to achieve this by assuming that each voxel in the 3D-OAM image exhibits a single chromophore contributing to the optoacoustic signal. The device is powered by a single optical source (SuperK Compact, NKT Photonics) that operates across an ultra-wide spectral range of 450 to 2400 nm. The set-up was optimized by minimizing optical aberrations and attenuation on optical components to stimulate the sample effectively. Using optical pulses of 2 ns duration and a repetition rate of 20 kHz, the device imaged tadpoles in their embryonic stage at multiple wavelengths, using narrow spectral windows of 25 nm bandwidth within the broad spectrum of the supercontinuum source at a time.

In addition, an ultra-high-resolution OCT imaging channel operating at 1300 nm (spectral bandwidth 180 nm) was created and incorporated into the device. The OCT channel, also powered by a commercial supercontinuum source (SuperK EXTREME EXR9, NKT Photonics), was used for guidance purposes and to help determine the location of the chromophores.

Keywords: optoacoustic microscopy, optical coherence tomography, multimodality imaging, tadpoles

1. INTRODUCTION

Optoacoustic Microscopy (OAM) is a cutting-edge imaging technique that provides high-resolution volumetric information on the structure and function of biological tissues. It allows for non-invasive detection of chromophores, making it an attractive option for a wide range of medical, oncological, and research applications in biology and neurosciences. However, typical OAM instruments have limited spectral capabilities and can only operate over narrow ranges; hence, only a few chromophores can be identified, posing a challenge in producing OAM maps of multiple biological chromophores.

Despite these limitations, some research groups have successfully demonstrated OAM's ability to produce maps of specific chromophores. For example, using three laser lines, Liu et al. [1] used OAM to simultaneously measure the concentration of Hb, oxygen saturation, and blood flow speed. Using a single nanosecond pulsed laser at 532 nm and two stimulated Raman shifted pulses at 545 and 558 nm, Liu et al. successfully mapped the oxygen saturation *in vivo*. Thanks to the employment of a high numerical aperture acoustic lens, the imaging was performed using only ten nJ per pulse and without the need for data averaging. Galanzha et al. [2] employed *in-vivo* OAM flow cytometry to detect melanin-bearing circulating tumor cells in melanoma patients. They utilized a pulsed laser operating at 1060 nm.

The broad spectral coverage offered by supercontinuum (SC) optical sources makes them an excellent choice for multi-spectral optical absorption (OA) imaging and spectroscopic OA sensing. However, their low pulse energy can pose a challenge. To address this, Shu et al. [3] developed a single SC source-powered OCT/OAM instrument equipped with multi-spectral microscopy (MS-OAM) capabilities in the visible range (500-800 nm). At the same time, Buma et al. [4] and Dasa et al. [5] created custom SC sources for mapping lipids in the near-infrared (NIR) range. This underscores the importance of matching imaging instruments to the spectral characteristics of the chromophore under investigation. Several other research groups have endeavored to create low-cost OAM imaging instruments. Pulsed laser diodes have been utilized in the visible and NIR regions to accomplish a specific objective. However, instruments that rely on pulsed laser diodes operate at a low pulse repetition rate and, as a result, a slow imaging rate. In addition, the signals detected need to be averaged hundreds of times to detect the low-energy pulses. Other methods include frequency-domain (FD) systems. For instance, Kellnberger et al. [6] employed a CW laser (at 488 and 808 nm), while Tserevelakis et al. [7] used a CW laser (at 488 nm) with an acousto-optic modulator at 10 MHz. In contrast to PLD-based OAMs and FD CW laser-based systems, Allen et al. [8] reported a more expensive ultra-fast OAM system with a pulse repetition rate (PRR) of 2 MHz using a master oscillator power amplifier configuration, frequency-doubled to 532 nm. Optical parametric oscillators (OPOs) are prevalent optical sources used for PAM, but despite their wide wavelength tunability, they are characterized by a low PRR.

Recently, Dasa et al. [5] released a study detailing their successful lipid mapping using a low-cost, custom-designed SC source in the near-infrared (NIR) range. In contrast, Bondu et al. demonstrated an OAM instrument employing an SC source operating in the visible range [9]. However, a cost-effective optical source that meets all the criteria for OAM imaging has yet to be developed, including coverage of both the visible (VIS) and NIR ranges, a high energy delivery, and a high pulse repetition rate (PRR) for efficient imaging.

In our research, we utilized a cost-effective and readily available SC source that emits light across a broad range of wavelengths, ranging from 450 to 2400 nm. With this source, we developed an imaging device that can identify a variety of chromophores, including melanin, hemoglobin (Hb), collagen, glucose, and lipids. This imaging technology is truly pioneering, as it can generate real-time 3D maps of different chromophores across the electromagnetic spectrum of the light emitted by this source. To create an even more advanced multimodal imaging instrument (OAM/OCT), we combined the OS-OAM with a high-resolution Optical Coherence Tomography (OCT) imaging channel.

2. METHODOLOGY

2.1 The experimental set-up

Figure 1 presents a schematic diagram of the multi-modal OS-PAM/OCT imaging instrument comprising two channels.

(a) **The OS-OAM channel**. In this channel, a supercontinuum source (SKC, SuperK COMPACT, NKT Photonics) delivers pulses of 2 ns duration and 20 kHz pulse repetition rate. To improve the lateral resolution of the images produced as well as increase the optical fluence on the sample, hence better signal-to-noise ratio, a beam-expander was used at the output of the SKC (not shown in Fig. 1). It is essential to keep in mind that the SKC source produces beams of varying sizes depending on the operating wavelength. The beam measures 1 mm in the visible but can increase to 3 mm in the near-infrared region. This means the captured images will exhibit unique characteristics based on the source's wavelength. After being expanded, the optical beam is spectrally filtered by the optical filter F and conveyed towards a galvo-scanner head GXY via a flipping mirror FM, which is employed to switch the operation of the instrument between the two imaging modalities (OCT or OAM). A high numerical aperture microscope objective is then used to focus light on the sample submerged in the aqueous solution. The ultrasonic transducer UT (40.3 MHz center frequency, University of Southern California), also immersed in the aqueous solution, converts the acoustic signal into an electrical one, which is then sampled by a high-speed digitizer (DAQ1, National Instruments, model PCI-5124). Before digitization, the electric signal is amplified by a sequence of two amplifiers (Mini-Circuits, model ZFL-500LN+) connected in series.

(b) **The OCT channel**. Light from a supercontinuum laser (EXR9, SuperK EXTREME EXR9, NKT Photonics) operating at 78 MHz is employed in this channel. After the EXR9, a SuperK Gauss filter (NKT Photonics) adjusts the spectrum to a near-gaussian shape centered at 1,300 nm. A directional coupler (DC) is then used to convey half of the optical power toward the sample via GXY and the other half toward the reference arm of the interferometer. Interference occurs in DC between the light back-scattered by the sample and the light back-reflected by the reference mirror M placed on the translation stage TS. The spectrometer employed here included

a transmission diffraction grading TG (Wasatch Photonics) and a linear camera (Goodrich, model SU1014-LDH), which can operate at a maximum acquisition rate of 47 kHz. Data conveyed via a camera link cable is digitized by an IMAQ board (National Instruments, model 1429). The display of B-scan OCT and PAM images is performed in real time. The generation of the PAM A-scans does not involve complex mathematical operations (a Hilbert transform is applied to each acquired temporal signal). Hence, the real-time display of the images is straightforward. The OCT channel is powered by the Master-Slave procedure [10-12], which allows for generating direct *en-face* views without data resampling. An in-house LabVIEW software was developed to drive the acquisition and the analysis procedure. Thus, the PCI-5124 digitizer was employed to digitize the electrical signal generated by the ultrasound transducer in synchronism with the pulses generated by SKC. A-scans from the signals generated by both OAM and the OCT channels are produced for each beam position on the sample.

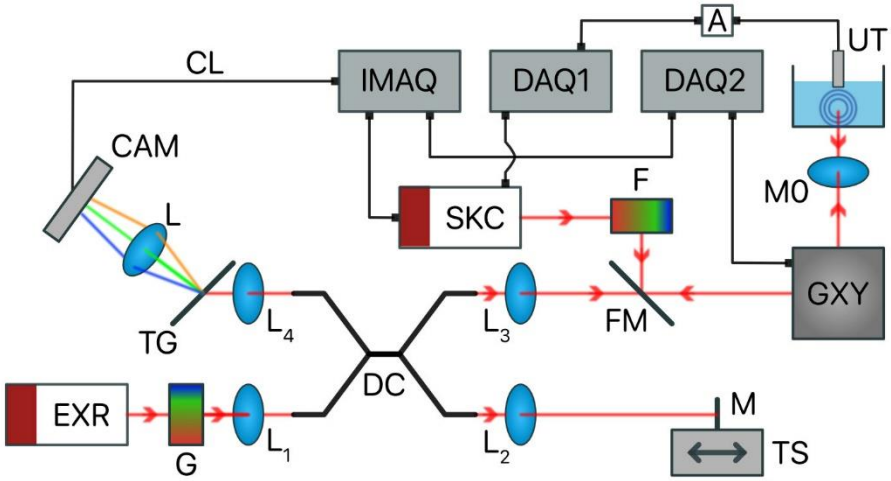


Figure 1. Schematic diagram of the OS-OAM/OCT instrument. SKC: OAM excitation optical source (SuperK COMPACT, NKT Photonics), EXR: OCT optical source (SuperK EXTREME EXR9, NKT Photonics), G Variable filter (SuperK GAUSS, NKT Photonics), F: bandpass filter wheel, FM: Flipping mirror, GXY: orthogonal galvanometer mirrors; CAM: linear camera; TG: transmission diffraction grating, DC 50/50 directional coupler, UT: ultrasound transducer, L, L_1–L_4 achromatic collimators, MO: microscope objective; M: flat mirror, A: amplifier; DAQ1: fast digitizer (NI, PCI5124), DAQ2: multifunctional I/O card used to drive the galvo-scanners (NI, PCI-6110); MO: microscope objective.

2.2 Theoretical approach

The theoretical model we developed to calculate the concentrations of the chromophores is based on the supposition that, for a given wavelength (or narrow spectral range), only one chromophore contributes to the brightness of a pixel in the OAM image [13]. Thus, by computing the difference between two images generated at two different wavelengths, we can determine which chromophores are present at each location in the image. Let us imagine that we are investigating the presence of two chromophores, A and B. If, for a pixel in the image, the difference between the pixel's brightness measured at two wavelengths (proportional to the difference between the initial pressures δp) is positive, the chromophore contributing to the signal is A. On the contrary, if the difference δp is negative, the contributing chromophore is B. If in a pixel of the OAM image, we have contributions from both melanin and Hb, when switching from 550 to 650 nm, we do expect an increase of the initial pressure due to the melanin and a decrease of the initial pressure due to the Hb (due to the strong absorption of the Hb at 550 nm and of the melanin at 650 m). Now, if we suppose that from a single point, we have either the signal from Hb or melanin, then $\delta p > 0$ indicates the presence of the Hb, whereas $\delta p < 0$ indicates that of the melanin. By carefully selecting the operation wavelength of the instrument, various chromophores can be mapped in the OAM image. Spectral ranges around 1200, 1600, and 1700 nm can be used to map glucose, collagen, and lipids.

3.1 System characterization

The OAM system was rigorously characterized; the results are presented in Figs. 2 and 3. The energy per pulse was measured on the sample for each wavelength and was found to range from 20 to 110 nJ (Fig. 2A). The lateral field of view

was estimated by imaging a carbon fiber tape demonstrating strong optoacoustic signal amplitude over 8 mm (Fig. 2B). As the lateral resolution varies with the wavelength and the beam diameter it is necessary to be measured for each wavelength. Thus, a sharp edge of a USAF target (a letter on the USAF target) was imaged for each wavelength. Images of 500×400 pixels^2 were produced of size 500×400 μm^2 therefore, each pixel in the image spans over 1 μm.

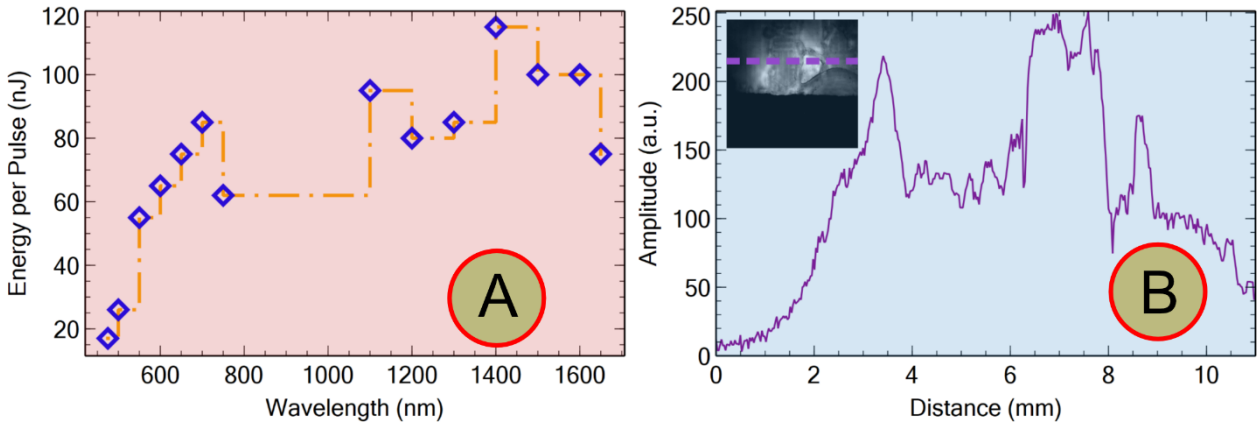


Figure 2. A. Experimental values of the energy per pulse (nJ) across imaging spectral range. B. Measurement of the lateral field of view of the instrument. The signal was collected while imaging a carbon fiber tape (along the dashed line shown in the inset image; the image size is 10×10 mm).

The edge and line spread functions (ESF in the inset presented in Fig. 3A) were measured, and the FWHM of the Gaussian fit to the line spread function (LSF in the inset presented in Fig. 3A) determined the lateral resolution. The measured lateral resolution was found to vary from 4.9 to 7.1 μm over a spectral range from 475 to 1650 nm. This range of variation in the lateral resolution is expected due to the variation of the beam diameter at the output of the optical source as a function of wavelength. The beam diameter at the output of the optical source is a function of wavelength. The theoretical lateral resolution of the instrument was calculated to be 5.8 μm at 500 nm and 6.95 μm at 1500 nm. These values match the experimental values and ensure that the achromat lens employed did not introduce optical aberrations. The theoretical axial resolution of the OAM instrument is 38 μm. However, the SNR is weaker outside the acoustic focal point, and the axial resolution degrades. Furthermore, the transducer has a maximum detectable bandwidth when it is oriented orthogonal to the direction of propagation of the incident acoustic waves. Any slight deviation of the incidence angle from 90 degrees, due to the angle directivity dependence, determines a reduction in the detectable signal bandwidth. Hence, the measured axial resolution using the carbon fiber tubes (Fig. 3B) results as 50 μm. The ratio between the max signal amplitude and the noise's standard deviation determines the OAM system's SNR, found to be 43.8 dB.

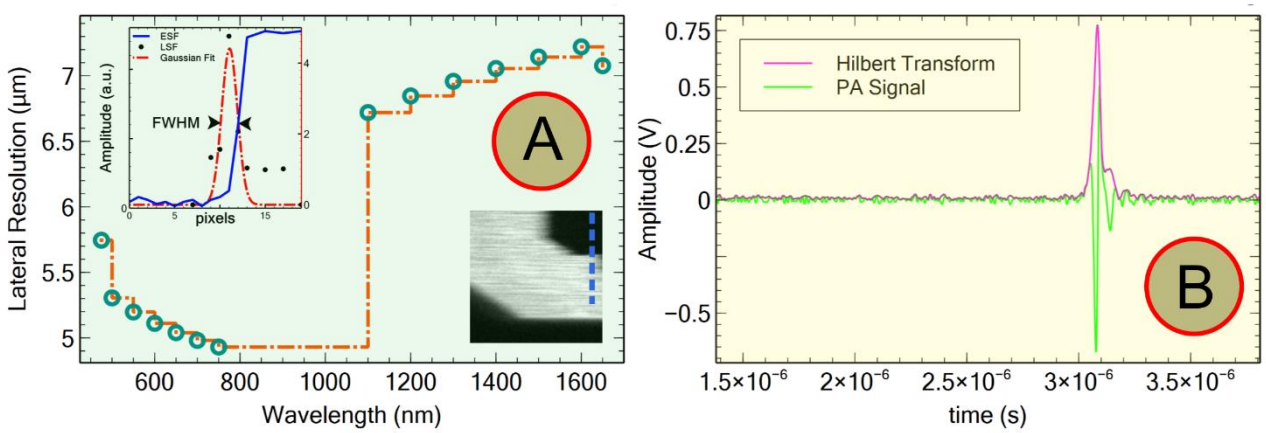


Figure 3. A. Experimental values of the lateral resolution across the spectral range performed by imaging a sharp edge of a character on a USAF target (image in the inset; the size of the image is 0.5×0.5 mm) B. Measurement of the axial resolution obtained by imaging a carbon fiber tape. We define the axial resolution as the FWHM of the photo-acoustic (PA) signal envelope.

3.2 Imaging of Xenopus Laevis

Four Xenopus laevis tadpoles at development stage 37/38 underwent imaging as part of a study that received approval from the University of Kent Animal Welfare and Ethical Review Body, with Institutional Ethics Reference Number 0037-SK-17. Before imaging, the tadpoles were anesthetized in 0.1% MS-222 solution. Throughout the entire 4.2-minute imaging procedure, they were kept anesthetized in MS-222 solution [14]. All methods used adhered strictly to the guidelines and regulations outlined in the research protocol approved by the University of Kent.

Our findings are summarised by the images presented in Fig. 4, produced using the OAM/OCT instrument we developed in combination with the technique described in the previous section. The first image (left, top) is a structural OCT image. The other images show maps of five endogenous contrast agents: melanin, Hb, collagen, glucose, and lipids in the tadpole's body. The images of the tadpole's OAM are superimposed on its corresponding structural OCT images. The maps of melanin were generated using filters (F) set at 550 and 650 nm. At the developmental stage 37/38 of the tadpole, pigmentation (caused by pigment cells) was observed in the eye, on the head, and the dorsal side of the yolk sac. Additionally, melanophores were found on the tail, indicated by a less intense melanin signal. Maps were generated for Hb using filters that operate at 550 nm and 650 nm. Hb was observed in the cardiac ventricle and along the vascular system that extends from the yolk sac and runs along the tail. Filters operating at 1200 nm and 1700 nm were used to obtain maps for collagen. Collagen was detected in various areas of the tadpole's body, including the developing cranial structures, yolk sac, and trunk muscles. Glucose mapping was carried out using images produced at 1600 and 1700 nm wavelengths. The yolk sac region showed high levels of glucose (Fig. 4), which overlapped with the high concentration of lipoproteins in that area. Furthermore, we mapped lipids using filters at 1200 and 1600 nm wavelengths. Our findings reveal that lipids are highly concentrated in the yolk sac region (Fig. 4), consistent with previous studies that employed multi-spectral OAM imaging of zebrafish and tadpoles.



Figure 4. These high-quality visuals showcase the distribution of melanin (pink), hemoglobin (magenta), collagen (green), glucose (yellow), and lipids (blue) throughout a tadpole. We generated these images by superimposing chromophore maps onto a structural OCT en-face image of the same tadpole. On the left, you can see the original OCT image of the tadpole, which served as the foundation for the chromophore maps.

3. CONCLUSIONS

This study demonstrated an OAM imaging instrument that operates at wavelengths ranging from 475 to 2400 nm. It also introduced a unique technique for mapping absorbers, which relied on the assumption that only one chromophore contributed to the photo-acoustic signal of each voxel in the 3D PAM image. This innovative approach allowed us to map five endogenous contrast agents in living tadpoles. Additionally, an ultrahigh-resolution OCT imaging channel was utilized to aid the investigation. Utilizing a specialized Supercontinuum optical source and optical set-up design has proven to be a highly effective technique for detecting chromophores. When designing the instrument, it was crucial to consider the absorption coefficient of a chromophore at a specific wavelength and the source's fluence and spectral density variation. Therefore, careful consideration was needed when selecting the two interrogation wavelengths. However, it is essential to note that the spectral range between 700 to 1100 nm, while of interest for biomedical applications, cannot be targeted by OAM due to the low absorption of chromophores. To maintain cost-effectiveness, measurements were not taken within this range. Even though more advanced systems can provide accurate absorption coefficient data, they are limited to only two chromophores due to a lack of spectral coverage or cannot perform *in-vivo* imaging due to the lack of imaging speed.

4. ACKNOWLEDGMENTS

GN and GM thank the University of Kent for its support. AP and AB acknowledge the support of the Biological Sciences Research Council (BBSRC), "5DHiResE" project, BB/S016643/1; AP also acknowledges the European Union's Horizon 2020 research and innovation program under the Marie Sklodowska-Curie grant NETLAS (agreement No 860807) and the National Institute for Health Research Biomedical Research Centre at Moorfields Eye Hospital NHS Foundation Trust (NIHR), the UCL Institute of Ophthalmology, University College London (AP) and the Royal Society Wolfson research merit award. SK acknowledges the support from The Physiological Society UK (Research Grant 2019). CM acknowledges financial support from the Multi-BRAIN project funded by the Lundbeck Foundation (R276-2018-869) and Villum Fonden (36063). MKD and OB acknowledge support from the Innovation Fund Denmark (4107-00011A) and the European Union's Horizon 2020 research and innovation program under the Marie Sklodowska-Curie grant (agreement No 722380). AB acknowledges the support of the Royal Society, project PARSOCT, RGS/R1/221324, and support of the Academy of Medical Sciences/the Wellcome Trust/the Government Department of Business, Energy and Industrial Strategy/the British Heart Foundation/Diabetes UK Springboard Award SBF007\100162.

REFERENCES

[1] Liu, C., Liang, Y. and Wang, L., "Single-shot photoacoustic microscopy of hemoglobin concentration, oxygen saturation, and blood flow in sub-microseconds," Photoacoustics **17**, 100156 (2020).
[2] Galanzha, E. I. et al., "In vivo liquid biopsy using Cytophone platform for photoacoustic detection of circulating tumor cells in patients with melanoma," Sci. Transl. Medicine **11** (2019).
[3] Shu, X. et al., "Single all-fiber-based nanosecond-pulsed supercontinuum source for multispectral photoacoustic microscopy and optical coherence tomography," Opt. Lett. **41**, 2743–2746 (2016).
[4] Buma, T., Conley, N. C., and Choi, S. W., "Multispectral photoacoustic microscopy of lipids using a pulsed supercontinuum laser," Biomed. Opt. Express **9**, 276 (2018).
[5] Dasa, M. K., Nteroli, G., Bowen, P., Messa, G., Feng, Y., Petersen, C.R., Koutsikou, S., Bondu, M., Moselund, P.M., Podoleanu, A., Bradu, A., Markos, C., and Bang, O., "All-fibre supercontinuum laser for in vivo multispectral photoacoustic microscopy of lipids in the extended near-infrared region," Photoacoustics **18**, 100163 (2020).
[6] Kellnberger, S. et al., "Optoacoustic microscopy at multiple discrete frequencies," Light. Sci. & Appl. **7**, 109 (2018).
[7] Tserevelakis, G. J., Mavrakis, K. G., Kakakios, N. & Zacharakis, G. Full image reconstruction in frequency-domain Photoacoustic microscopy by means of a low-cost I/Q demodulator. Opt. Lett. **46**, 4718–4721, (2021).
[8] Allen, T., Spurrell, J., Berendt, M.O., Ogunlade, O., Alam, S.U., Zhang, E.Z., Richardson, D.J., and Beard, P.C., "Ultrafast laser-scanning optical-resolution photoacoustic microscopy at up to 2 million A-lines per second," Journal of Biomedical Optics **23**, 126502 (2018).
[9] Bondu, M., Marques, M.J., Moselund, P.M., Lall, G., Bradu, A., and Podoleanu, A., "Multispectral photoacoustic microscopy and optical coherence tomography using a single supercontinuum source," Photoacoustics, **9**, 2213-5979, (2018).
[10] Podoleanu, A. G., and Bradu, A., "Master-slave interferometry for parallel spectral domain interferometry sensing and versatile 3D optical coherence tomography," Opt. Express **21**, 19324–19338 (2013).
[11] Bradu, A., Israelsen, N.M., Maria, M., Marques, M.J., Rivet, S., Feuchter, T., Bang, O., and Podoleanu, A., "Recovering distance information in spectral domain interferometry," Scientific Reports **8**, 15445 (2018).
[12] Bradu, A., Rivet, S., and Podoleanu, A., Master/slave interferometry – ideal tool for coherence revival swept source optical coherence tomography, Biomed. Opt. Express **7**, 2453-2468 (2016).
[13] Nteroli, G., Dasa, M.K., Messa, G., Koutsikou, S., Bondu, M., Moselund, P.M., Markos, C., Bang, O., Podoleanu, A., and Bradu, A., "Two octaves spanning photoacoustic microscopy," Sci Rep. **12**, 10590 (2022).
[14] Koutsikou, S. et al., "A simple decision to move in response to touch reveals basic sensory memory and mechanisms for variable response times," The J. Physiol. **596**, 6219–6233 (2018).